A&A 441, 1031–1038 (2005)
DOI: 10.1051/0004-6361:20053118

Astronomy & Astrophysics

The orbiting gas disk in the Red Rectangle⋆,⋆⋆

V. Bujarrabal[1], A. Castro-Carrizo[2], J. Alcolea[3], and R. Neri[2]

[1] Observatorio Astronómico Nacional, Apartado 112, 28803 Alcalá de Henares, Spain
e-mail: v.bujarrabal@oan.es
[2] IRAM, 300 rue de la Piscine, 38406 St.-Martin-d'Hères, France
e-mail: ccarrizo@iram.fr, neri@iram.fr
[3] Observatorio Astronómico Nacional, C/Alfonso XII, 3, 28014 Madrid, Spain
e-mail: j.alcolea@oan.es

Received 23 March 2005 / Accepted 26 April 2005

ABSTRACT

We present accurate maps of the CO J = 2–1 and 1–0 lines made with the Plateau de Bure interferometer of the gas disk around the central star(s) of the Red Rectangle, a well known protoplanetary nebula. We confirm that the molecular gas in this source forms a disk perpendicular to the conspicuous axis of symmetry of the optical nebula and that this disk is in rotation. We present detailed modeling of the CO emission and extensive discussion of the accuracy of the values fitted for the different parameters. The outer radius of the disk is $\sim 2.7 \times 10^{16}$ ($\frac{D(\mathrm{pc})}{710}$) cm, as a function of the assumed distance D, which is thought to vary between 380 and 710 pc. The rotation is found to be Keplerian, at least in the inner disk. From this velocity field, we derive a central mass between 0.9 $M_\odot$, for a distance of 380 pc, and 1.7 $M_\odot$, for 710 pc. Previous studies of the nature of the stellar component favor the highest values. In the outer disk, we deduce the presence of a slow expansion velocity ($\sim$0.8 km s^{-1}), superimposed on rotation. We find gas temperatures decreasing from $\sim$400 to 30 K across the disk and densities $\gtrsim 3 \times 10^4$ cm^{-3}.

Key words. stars: AGB and post-AGB – stars: circumstellar matter – radio-lines: stars – planetary nebulae: individual: Red Rectangle

1. Introduction

The existence of gas disks orbiting post-AGB stars has been postulated several times, often associated with the presence of a stellar or substellar companion, in order to explain the very energetic axial outflows that take place in this evolutionary phase (see Soker 2002; Frank & Blackman 2004, and references therein). Planetary and protoplanetary nebulae (PNe, PPNe) very often show axisymmetric shapes and fast axial movements, which are thought to be due to shock interaction between the very collimated post-AGB jets and the slow and isotropic AGB wind. According to simulations (e.g. Frank & Blackman 2004), accretion from disks rotating around post-AGB stars (in the presence of a bipolar magnetic field) can provide the energy and momentum required to explain the PPN dynamics via the ejection of very fast jets. The actual presence of rotating disks around post-AGB stars is therefore a basic question in order to understand the post-AGB ejections, and therefore the spectacular and very fast evolution of the shape and dynamics of PPNe.

Disks/tori of molecular gas around post-AGB stars are commonly detected as the central part of protoplanetary nebulae, although they are not observed to rotate, but to be systematically in expansion (like the rest of the nebula). Such expanding structures are usually thought to be mere remnants of the former AGB winds. See the cases of M 1–92 (Bujarrabal et al. 1998), M 2–9 (Zweigle et al. 1997), M 2–56 (Castro-Carrizo et al. 2002), etc.

The Red Rectangle is the only PPN in which a central disk has been actually observed in rotation (Bujarrabal et al. 2003, Paper I), from CO J = 2–1 and J = 1–0 line maps. In spite of their relatively poor resolution (worse than $\sim$2 arcsec), these maps and in particular the velocity–position brightness distributions suggested the presence of a rotating gas disk perpendicular to the optical nebula axis. Modeling of the data supported the idea that the rotation is Keplerian, at least in the inner disk, and therefore that this component is relatively stable. The data also suggested that a slow expansion velocity ($\sim$0.6 km s^{-1}) may be superimposed on the rotation in the outer disk.

The Red Rectangle is a well known PPN that surrounds the A1 star HD 44179, a spectroscopic binary (e.g. Waelkens et al. 1996). The optical nebula is very extended (about 1′) and presents a conspicuous axis of symmetry. The orientation of this axis slightly varies from small-scale to large-scale images

⋆ Based on observations carried out with the IRAM Plateau de Bure Interferometer. IRAM is supported by INSU/CNRS (France), MPG (Germany) and IGN (Spain).
⋆⋆ Appendix is only available in electronic form at http://www.edpsciences.org

around a position angle ∼11° (see Roddier et al. 1995; López et al. 1995; Tuthill et al. 2002; Cohen et al. 2004). The presence of orbiting material in the Red Rectangle was proposed to explain several properties of this object, like the probable presence of big grains and the anomalous abundances found in the stellar atmosphere, but without any direct detection (see e.g. Waelkens et al. 1996; Jura et al. 1995, 1997; and Paper I). Following similar arguments, disks have also been proposed for a few other evolved stars (see Waters et al. 1992; Jura & Kahane 1999, etc.)

In this paper, we present observations of ^{12}CO line emission from the Red Rectangle with an angular resolution better than 1″. We have also significantly improved the signal-to-noise ratio of the maps, particularly in the J = 1–0 line. As we will see, the high quality of the data allows a much more detailed modeling, and the significance of the derived parameter values is largely improved. We confirm both that the CO-rich gas is confined in an equatorial disk and the dynamics depicted above.

2. Observations

We observed the Red Rectangle in the rotational transitions ^{12}CO J = 2–1 at 1.3 mm wavelength (230.538 GHz) and ^{12}CO J = 1–0 at 2.6 mm (115.271 GHz) with the IRAM six-element array at Plateau de Bure. The 15 m antennas are all equipped with dual-band SIS receivers yielding SSB receiver temperatures of 40 K at 2.6 mm and 60 K at 1.3 mm. Observations were performed in January and February 2004 in excellent atmospheric conditions (≃1 mm of precipitable water vapor) and in the array's AB set of configurations. Projected baselines range from 408 m to 15 m. The ^{12}CO lines were observed with 20 MHz correlator units providing a nominal resolution of 0.05 km s^{-1} at 1.3 mm (0.1 km s^{-1} at 2.6 mm) and a velocity coverage of ≃23 km s^{-1} at 1.3 mm (≃46 km s^{-1} at 2.6 mm). These setups were used to produce line maps with an effective velocity resolution of 0.6 km s^{-1}. The continuum emission was observed with 320 MHz correlator units adjusted to match the full frequency coverage of the receivers. A sensitivity of 0.5 mJy beam^{-1} was achieved at 2.6 mm with a 500 MHz line-free bandwidth, and of 0.6 mJy beam^{-1} at 1.3 mm with a 1080 MHz line-free SSB-equivalent bandwidth. The radio source 0420−014 was used as a bandpass calibrator, 0607−157 and 0727−115 as amplitude and phase calibrators, and MWC 349, 3C 84, AFGL 618 and 3C 454.3 to bootstrap the flux density scale. The data reduction was performed in the standard antenna-based mode using the GILDAS software. Systematic and statistical uncertainties in the absolute flux calibration were found to contribute by less than 10% at 2.6 mm and by 10% to 20% at 1.3 mm.

Figures 1 and 2 show the ^{12}CO J = 2–1 and J = 1–0 emission maps. The corresponding synthesized beams are plotted in each figure, and have a half-power size of 1.3 × 0.5 arcsec with a position angle (PA) of 14 degrees at 1.3 mm and of 2.6 × 1.0 arc seconds with a PA of 14 degrees at 2.6 mm. The conversion factors from main-beam temperature to flux density are 35.5 K per Jy beam^{-1} and 35.3 K per Jy beam^{-1} at 1.3 and 2.6 mm, respectively.

The continuum emission at 1.3 mm (see Fig. 1) shows a slightly resolved source of nearly gaussian shape peaking at RA $06^{h}19^{m}58\overset{s}{.}21$ and Dec $-10°38'14\overset{''}{.}8$ (J2000), with a full width at half-maximum of 1.4 × 0.8 arc seconds and a PA of 149 degrees. The main-beam temperature to flux density conversion factors are 34.6 K per Jy beam^{-1} and 35.9 K per Jy beam^{-1} at 1.3 and 2.6 mm, respectively. The continuum source shape and position are found to be in agreement with previous observations by Bujarrabal et al. (2003).

By comparison of the spectral profiles obtained from the integrated flux in our maps with the single-dish profiles observed at the 30 m telescope, we conclude that there is no flux lost in the 2.6 and 1.3 mm interferometric maps.

3. The distribution of the CO emission in the Red Rectangle

In Figs. 1 and 2 we show our maps per velocity channel of the CO J = 2–1 and J = 1–0 transitions, respectively. The J = 2–1 maps show the highest resolution, so we will often refer to them to derive the disk geometry. As we see, the CO emission comes from a structure elongated at position angle PA ∼ 101° (measured from north to east), which is interpreted as the projection of a disk almost perpendicular to the plane of the sky (Sect. 1). The observed brightness distribution is then accurately perpendicular to the prominent axis of the optical nebula, whose PA is equal to 11° (Sect. 1). To simplify the description, we will often refer to the direction of the elongated CO distribution in the plane of the sky as "the disk direction". The velocity–position diagrams along the CO disk are presented for both transitions in Fig. 3, together with the predictions of our nebula modeling (see Sect. 4). A diagram along the perpendicular direction (i.e. parallel to the axis of the optical nebula) is shown for the J = 2–1 line in Fig. 4. The total extent in the CO disk direction is found to be ∼5.″7 (without beam deconvolution).

In the direction perpendicular to the disk, we note that the sizes measured at the extreme velocities and at the central one are different (Figs. 1 and 4). At the extreme velocities, the measured extent in this direction is ∼1.″6, only slightly larger than the beam width (1.″32), indicating that the actual extent of the source is ∼0.″9. Note that in the very first and last panels in Fig. 1 only continuum emission is detected. At the central velocities we measure an extent at half-maximum ∼2″, which corresponds to an actual size of about 1.″5. As we will see in Sect. 4, this result is interpreted as showing that the disk thickness varies and is somewhat smaller in the inner regions rotating at the highest velocities.

Our maps of the CO J = 1–0 line have a poorer resolution than those of the J = 2–1 transition, but are significantly better than those presented in Paper I and are good enough to allow precise modeling (Sect. 4, Appendix A). As we will see, these data become necessary to model the density distribution, since the J = 1–0 line is less opaque than the J = 2–1 one.

The velocity distribution confirms our main result in Paper I: the molecular gas disk in the Red Rectangle is rotating around the central star. Our data indicate quite conclusively (we think) that at least the central part of the disk is in stable

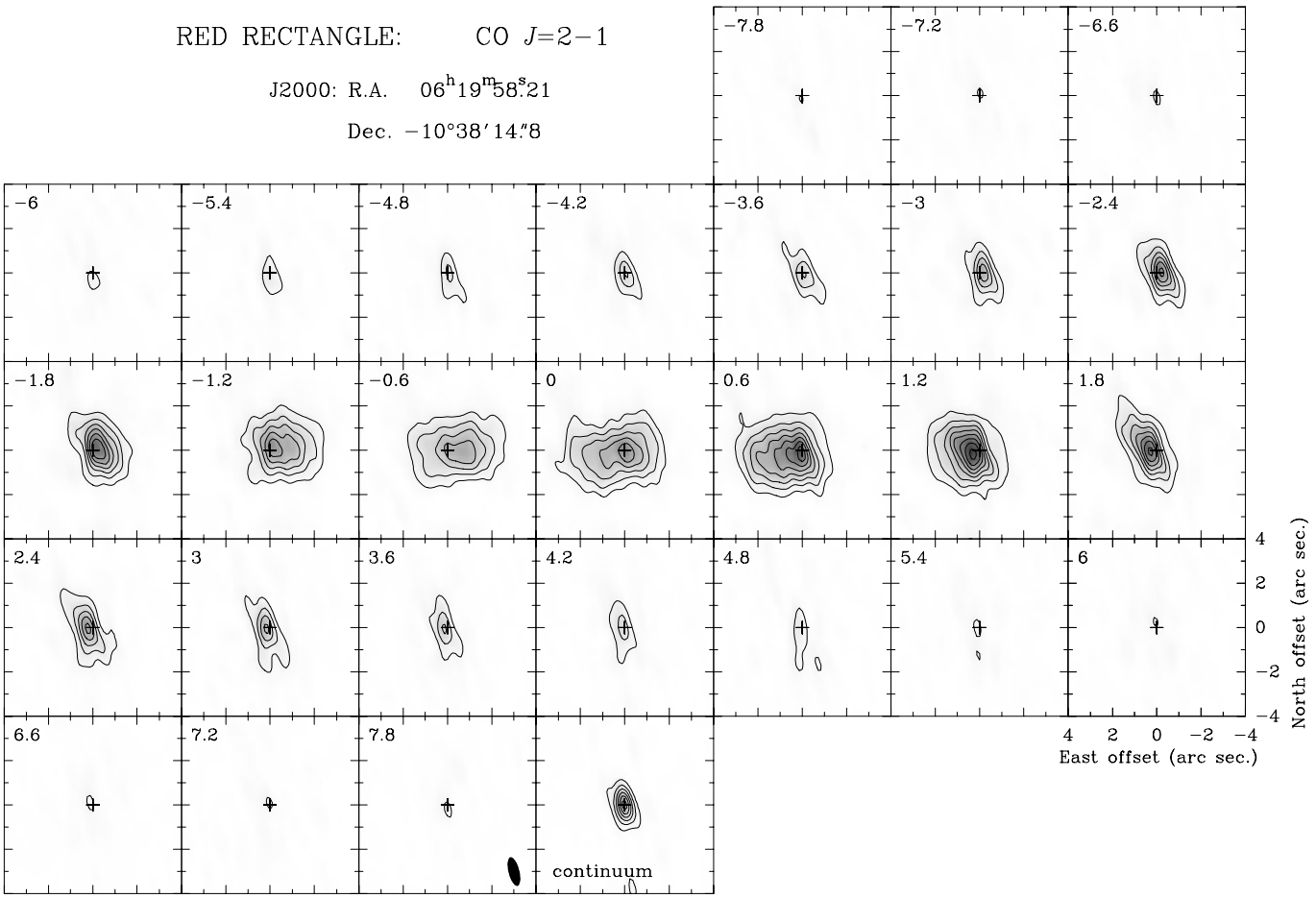

Fig. 1. Plateau de Bure maps of the Red Rectangle in CO J = 2–1 for a velocity resolution of 0.6 km s^{-1} (continuum not subtracted). The central LSR velocity (in km s^{-1}) of each channel map is indicated in the top-left corners. The first contour and the separation between contours is 0.2 Jy beam^{-1} (equivalent to 7.09 K in $T_{\rm mb}$ units). We also present the clean beam at half-maximum (black ellipse) and the continuum map (contour separation equal to 0.02 Jy beam^{-1}). The coordinate offsets are given with respect to the central position of the continuum, indicated in the figure.

Keplerian rotation, with its well known signature clearly present in the velocity–position diagram along the disk (Fig. 3).

As in previous CO data (Paper I), we note the presence of a significant asymmetry in our maps between positive and negative velocities, as the blue-shifted emission (between ∼0 and −1.5 km s^{-1} LSR) is weaker. We interpret this as due to absorption by the outermost disk parts, a phenomenon very often observed in circumstellar envelopes around AGB stars. For this effect to be possible, the rotation kinematics must be composed with expansion (in our case, a quite slow expansion, $\lesssim$1 km s^{-1}).

4. CO emission model

4.1. Description of the code and model parameters

In order to better extract the astrophysical information contained in our data, we used a nebula model similar to that presented in Paper I, where more details on the model can be found.

The continuum emission is treated in a more accurate way than in our previous work; note that its contribution is not subtracted from the maps. We assume the detected mm-wave continuum to be due to optically thin dust emission, since the measured intensities are compatible with the extrapolation of the FIR dust emission (e.g. Alcolea & Bujarrabal 1991). The spatial distribution of the dust emission coefficient is described in the code by a three-dimension gaussian function around the nebula center; the corresponding parameters are estimated from normalization of the resulting total flux and extent with respect to the data (Sect. 2). The dust emissivity is added to the line emission coefficient in the region in which continuum emission is found to originate, following the standard radiative transfer equations. Note that there is no link in our model between the dust emissivity distribution and the gas density one, since, in fact, the dust and CO emission maps are very different.

In the line emission model, the population of the CO rotational levels is given by a single excitation temperature, which is assumed to be equal to the kinetic temperature. As discussed in Paper I (see also Bujarrabal et al. 1997), these approximations are valid for the typical densities actually found from our model fitting ($\gtrsim 10^5$ cm^{-3}) and the high opacities expected for the CO lines. We assume a shape of the CO cloud and a spatial distribution of the velocity, temperature, density, and

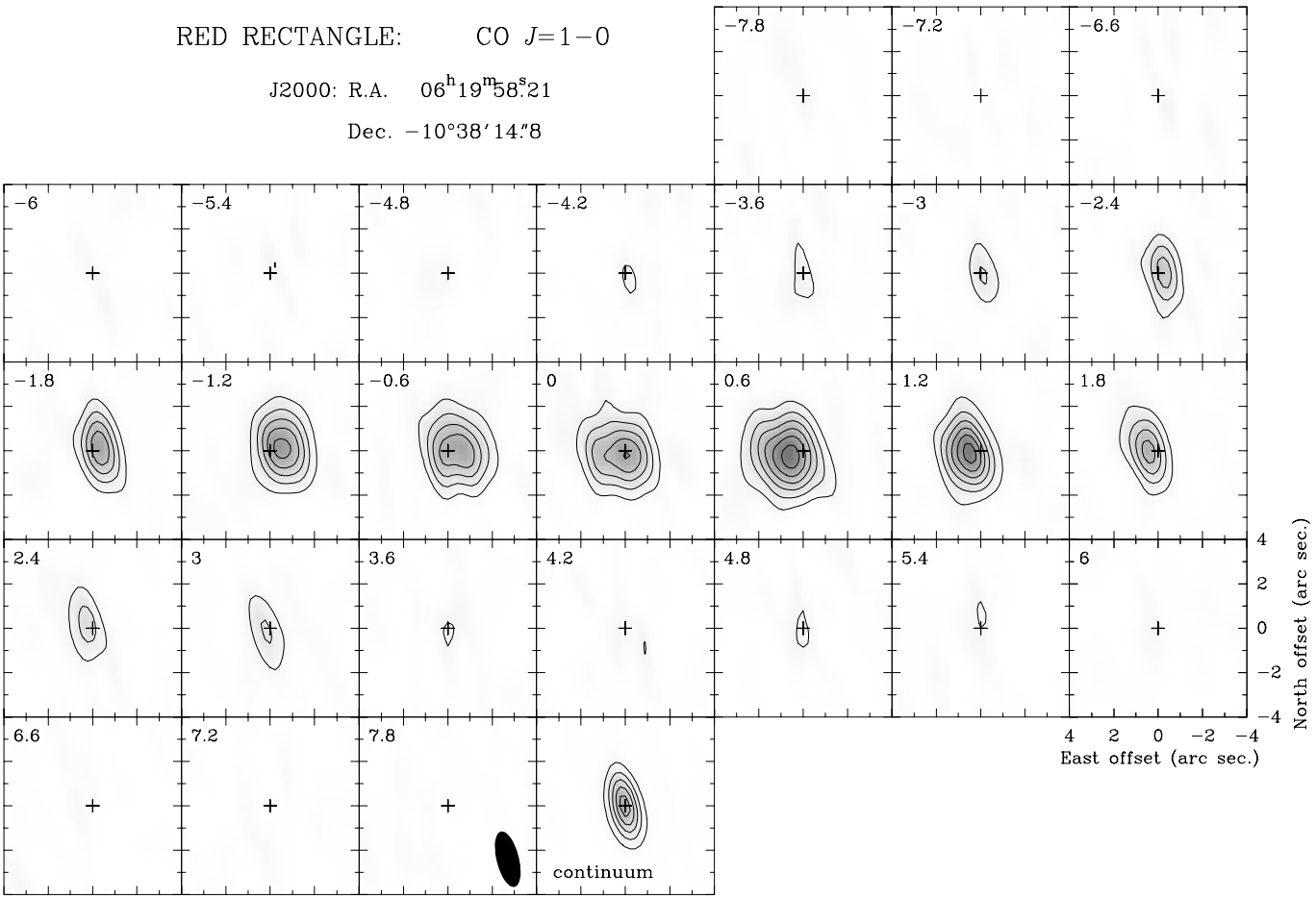

Fig. 2. Plateau de Bure maps of the Red Rectangle in CO J = 1–0 for a velocity resolution of 0.6 km s^{-1} (continuum not subtracted). The central LSR velocity (in km s^{-1}) of each channel map is indicated in the top-left corners. The first contour and the separation between contours is 0.1 Jy beam^{-1} (equivalent to 3.53 K in $T_{\rm mb}$ units). We also present the clean beam at half-maximum (black ellipse) and the continuum map (contour separation equal to 0.005 Jy beam^{-1}). The coordinate offsets are given with respect to the same central position as in Fig. 1.

CO relative abundance. Given these parameters, our code calculates the brightness for a number of lines of sight solving the full radiative transfer equation. Such a brightness distribution is convolved with the cleaned telescope beam, and images with the same units as the observed ones are produced.

The general features of the source geometry and kinematics are similar to those presented in Paper I, since the data in that paper are compatible with our new observations. CO emission is supposed to come from a rotating disk, in which expansion and turbulent movements can also be present. Axial symmetry is always assumed. We assume the distance to the Red Rectangle ranges between $D \sim 380$ pc, following the discussion in Paper I, and 710 pc, as proposed by Men'shchikov et al. (2002) from modeling of scattered light images and continuum emission. The straightforward scaling of the fitted parameter values with the distance is given in Sect. 4.2.

Some geometrical features are almost directly given by the observations, in particular from the high resolution maps of the J = 2–1 line, although in all cases their values have been checked to lead to model predictions compatible with the maps.

The position angle of the disk symmetry axis (measured from north to east) is assumed to be equal to that taken in Paper I, 11°. This value is confirmed by our high-resolution CO maps and agrees with the symmetry axis of the optical image (Sect. 1). From optical data, the inclination of the nebula axis with respect to the plane of the sky is known to be small but not negligible, ∼5° (see Paper I), with the southern lobe closer to us. Our maps are consistent with this small inclination angle, as we can see from the small difference between the measured thickness in the axial direction of the regions far from and close to the star in the central velocity channels (Fig. 1); these regions correspond, respectively, to the outermost disk regions (whose observed width is in the limit not affected by the projected disk size) and to the slowly rotating regions at projected positions close to that of the star (whose observed width should be more or less equal to the addition of the disk thickness and the projected disk size in the axial direction). Our model calculations also confirm this low value for the axis inclination with respect to the plane of the sky.

From the total extent of the observed disk (Sect. 3, see Figs. 1 and 3), the outer radius of the disk ($R_{\rm out}$) is found to be $\sim 2.7 \times 10^{16}$ cm, for a distance of 710 pc. The thickness of the disk H, which was poorly estimated in Paper I due to the relatively low resolution in that work, can be measured from our maps. H in the outer disk can be estimated from the disk thickness measured at the central velocities at large distances

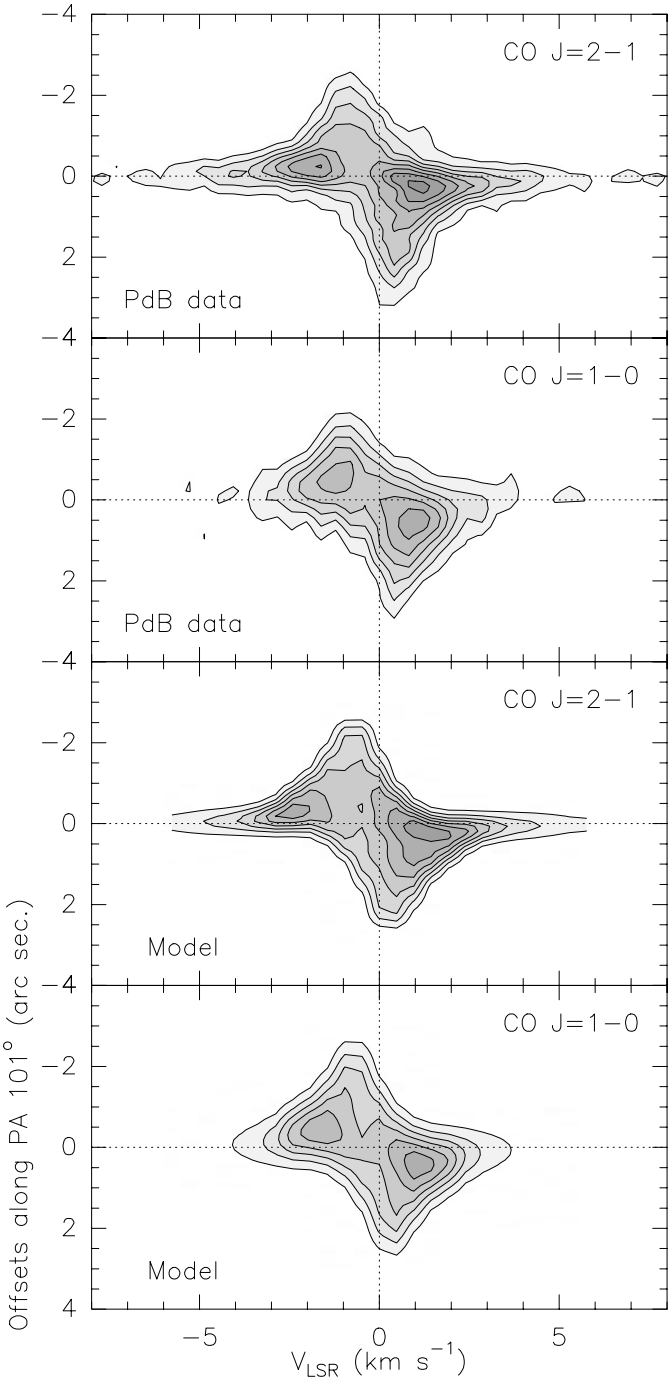

Fig. 3. Velocity–position diagrams of the CO $J = 2$–1 and $J = 1$–0 lines along the direction of the CO disk (at a position angle equal to 101°) and perpendicular to the axis of the optical image of the nebula. The lowest panels show the best theoretical fit from our model calculations. Contours are as in Figs. 1 and 2 for both observations and calculations. Continuum emission has not been subtracted and has been accounted for in our models.

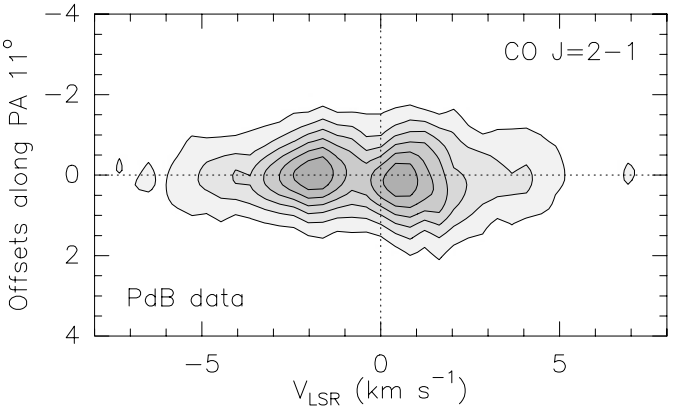

Fig. 4. Velocity–position diagram along the direction of the axis of the nebula (i.e. at position angle PA = 11°) of the CO $J = 2$–1 line. Contours are the same as in Figs. 1 and 3. Continuum emission has not been subtracted.

from the star, where the effects of the disk inclination are minimum. It is also possible to measure the extent from the maps at the extreme velocities, close to the stellar position, which should give the size of the innermost regions. The results from both methods are presented in Sect. 3. From those figures, we deduce that $H \sim 1.5 \times 10^{16}$ cm (for $D = 710$ pc) in outer disk regions. However, the directly measured thickness of the disk at the extreme velocities is significantly smaller, at least for projected velocity shifts $\gtrsim 2$ km s^{-1}. This implies that the actual thickness of these inner, rapidly rotating regions is smaller than the value previously obtained for the outermost regions. Due to the effects of the disk inclination and the small angles to be measured, the exact variation of H with r is difficult to determine. For the same reasons, the model fitting of the data is not accurate in this respect. To simplify the model, we accordingly assume a constant thickness H in regions farther than a certain radius and that H decreases with the distance to the axis in the innermost parts of the disk, down to one half of the maximum thickness. The radius delimiting both regions is imposed so as to be equal to the one used to separate the expanding-rotating disk from the Keplerian rotation ($R_{\rm kep}$, see below).

In the definition of the disk kinematics, the rotating disk is composed of two parts in our models. The inner disk is in Keplerian rotation, i.e. the tangential velocity is inversely proportional to the square root of the distance to the central star, $V_{\rm t} \propto 1/\sqrt{r}$. But, from a given distance to the central star, $R_{\rm kep}$, a low radial expansion velocity ($V_{\rm exp}$) appears, and the tangential velocity varies according to the law of angular momentum conservation ($V_{\rm t} \propto 1/r$). Such a law is expected for a rotating disk that shows a significant expansion and whose structure is more or less stable. $R_{\rm kep}$, $V_{\rm t}(R_{\rm kep})$ and $V_{\rm exp}(r)$ are free parameters of the model. Our code allows $V_{\rm exp}$ to vary with the distance for $r > R_{\rm kep}$. The model fitting of the data has not suggested the need of a jump in the rotational velocity at $R_{\rm kep}$.

The local velocity dispersion is assumed to be composed of the thermal dispersion (given by the kinetic temperature distribution, see below) and turbulent movements, whose velocity distribution is taken to be gaussian and described by its standard dispersion, $\sigma_{\rm turb}$, a free parameter of the model fitting.

The total density n and temperature T of the disk gas are assumed to vary with potential laws. Thus, in our model: $n(r) = n(R_{\rm kep})(R_{\rm kep}/r)^{\alpha_n}$ and $T(r) = T(R_{\rm kep})(R_{\rm kep}/r)^{\alpha_{\rm T}}$, where $n(R_{\rm kep})$, $T(R_{\rm kep})$, α_n, and $\alpha_{\rm T}$ are free parameters and can in principle be different for both Keplerian and expanding regions. However, we are trying to keep the model as simple as

Table 1. Structure and physical conditions in the molecular disk in the Red Rectangle, derived from our model fitting of the CO data. Dependence on the assumed distance is given in the relevant cases. Other parameters of the modeling are also given.

	Inner disk ($r < R_{\rm kep}$)		Outer disk ($r > R_{\rm kep}$)	
Parameter	Law	Values	Law	Values
Outer radius		$R_{\rm kep} = 8.4 \times 10^{15}$ ($\frac{D({\rm pc})}{710}$) cm		$R_{\rm out} = 2.7 \times 10^{16}$ ($\frac{D({\rm pc})}{710}$) cm
Disk thickness	linear	$H(R_{\rm kep}) = 1.5 \times 10^{16}$ ($\frac{D({\rm pc})}{710}$) cm $H(0) = 7.5 \times 10^{15}$ ($\frac{D({\rm pc})}{710}$) cm	constant	$H = 1.5 \times 10^{16}$ ($\frac{D({\rm pc})}{710}$) cm
Tangential velocity	$V_{\rm t} \propto 1/\sqrt{r}$ (Keplerian)	$V_{\rm t}(R_{\rm kep}) = 1.65$ km s^{-1} (central mass: 1.7 ($\frac{D({\rm pc})}{710}$) $M_\odot$)	$V_{\rm t} \propto 1/r$ (ang. mom. cons.)	$V_{\rm t}(R_{\rm kep}) = 1.65$ km s^{-1}
Expansion velocity		0 km s^{-1}	$V_{\rm exp} \propto \sqrt{a + b/r}$	$V_{\rm exp}(R_{\rm kep}) = 1.6$ km s^{-1} $V_{\rm exp}(R_{\rm out}) = 0$ km s^{-1}
Turbulence velocity	constant	$\sigma_{\rm turb} = 0.3$km s^{-1}	constant	$\sigma_{\rm turb} = 0.3$ km s^{-1}
Temperature	$T \propto 1/r^{\alpha_{\rm T}}$	$T(R_{\rm kep}) = 60$ K $\alpha_{\rm T} = 0.7$	$T \propto 1/r^{\alpha_{\rm T}}$	$T(R_{\rm kep}) = 76$ K $\alpha_{\rm T} = 0.7$
Gas density	$n \propto 1/r^{\alpha_n}$	$n(R_{\rm kep}) = 4 \times 10^5$ ($\frac{710}{D({\rm pc})}$) cm^{-3} $\alpha_n = 2.2$	$n \propto 1/r^{\alpha_n}$	$n(R_{\rm kep}) = 1.3 \times 10^5$ ($\frac{710}{D({\rm pc})}$) cm^{-3} $\alpha_n = 2.2$

Other parameters	Law	Values	Comments
Axis inclination from the plane of the sky		5°	from optical and CO data
Axis inclination in the plane of the sky (PA)		11°	from optical and CO data
Distance		between 380 and 710 pc	various arguments (Sect. 4)
CO relative abundance	constant	2×10^{-4}	from ^{12}CO and ^{13}CO data
LSR systemic velocity		-0.2 km s^{-1}	from CO data

possible, so the values of the above parameters are the same inside and outside $R_{\rm kep}$, unless absolutely imposed by the data fitting. These laws for the density and temperature are very similar to those found in circumstellar envelopes around AGB stars (e.g. Goldreich & Scoville 1976; Groenewegen et al. 1998; Schöier & Olofsson 2001).

We assume a CO relative abundance $X({\rm CO}) = 2{\times}10^{-4}$, usually found to be reasonable in PPNe and young PNe; see discussion in Paper I and Bujarrabal et al. (2001). Note that, due to the assumption of a thermalized level population, changes in the abundance and density are compensated for exactly in the model predictions when the product nX remains constant. See discussion of this assumed value in Appendix A.5.

4.2. Fitted values for the model parameters

The values of the parameters in the model that better fits our data are given in Table 1, where we also quote the values of other parameters discussed in Sect. 4.1 which affect the model calculations. In Fig. 3 we show the model predictions for our best fit, together with the observational results. The residuals of the fitting are presented in Fig. 5, using the same units and scales as in Fig. 3; the rms deviation from the observations is ∼5 K and the residuals are rarely higher than one contour. In the comparison of our synthetic maps with the data we take a systemic LSR velocity of ~ -0.2 km s^{-1}.

From the Keplerian velocity field deduced in our calculations, we can measure the central total mass (around which our disk rotates), which is found to be equal to 0.9 $M_\odot$, for a distance D = 380 pc (taken in Paper I), and equal to 1.7 $M_\odot$, for 710 pc (distance deduced by Men'shchikov et al. 2002). As far as the Keplerian rotation of the inner disk is well established and the distance between the two central stars (∼1 AU, e.g. Waelkens et al. 1996) is much smaller than the distances at which we find Keplerian orbiting, we think that this method for estimating the central mass is reliable. Both estimates are quite compatible with the stellar total mass found from the binary dynamics and stellar evolution considerations, which ranges precisely between 0.9 (Men'shchikov et al.) and 1.7 $M_\odot$ (Waelkens et al.). If we take into account the high mass of the very inner circumstellar shells in the model by Men'shchikov et al., the derived central mass is quite comparable to that found by Waelkens et al. Accordingly we conclude that the central mass is probably ∼1.7 $M_\odot$ (and $D \sim$ 710 pc). We note that both papers agree in concluding that a low-mass binary system is placed in the center of the Red Rectangle, although they diverge in their analyses of other properties of the stellar component. Further discussion of the nature of the central stellar system is beyond the scope of our work.

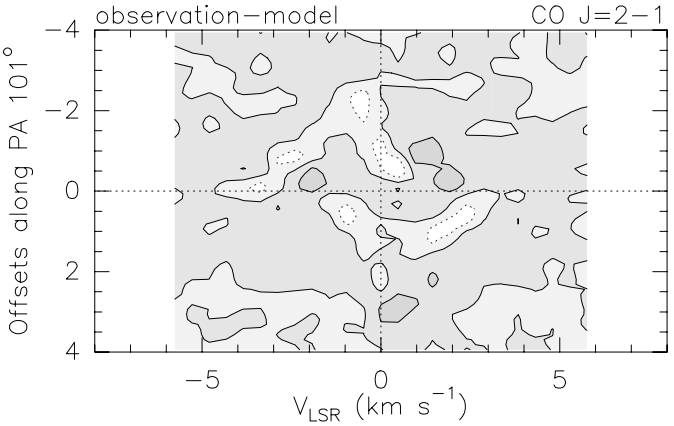

Fig. 5. Residuals of our model fitting of the observed CO $J = 2$–1 maps. We show a velocity–position diagram along the direction perpendicular to the axis of the optical image of the nebula, as in Fig. 3. Contours are −0.2 (dashed), 0, and 0.2 Jy beam^{-1}, with the same contour step as in Fig. 3.

The total mass of the model gas disk is equal to 3.5×10^{30} gr $= 2 \times 10^{-3}$ $M_\odot$ for $D = 380$ pc. For a distance equal to 710, the total disk mass is 6×10^{-3} $M_\odot$. Note that a jump in the density and temperature at $R_{\rm kep}$ is necessary to fit the data (Appendix A).

As mentioned in Sect. 4.1, determination of the distance is uncertain. The parameter values deduced from the model fitting scale easily with distance. For instance, the central stellar mass and the nebular linear sizes vary with D, the density varies $\propto 1/D$, and the total gas mass varies with D^2. In the laws deduced for the different parameters, we must scale r with D. The temperature and velocities only vary following this scaling of the laws.

5. Conclusions

We present interferometric maps of the CO $J = 2$–1 and 1–0 lines made with the Plateau de Bure interferometer of the gas disk around the central star(s) of the Red Rectangle. These new accurate observations, with high spatial and spectral resolution and high signal-to-noise ratio, confirm our previous claim (Bujarrabal et al. 2003, Paper I) that the molecular gas in this source forms a disk perpendicular to the conspicuous axis of symmetry of the optical nebula and that this disk is in rotation around the central star. We performed detailed modeling of the line emission of the source, in order to better determine its structure, velocity field and physical conditions. We present in Sect. 4 a detailed discussion of the model, the method to derive the values of the different model parameters, and the accuracy of each of these values (see also the Appendix). The parameters and fitted values are summarized in Table 1.

We have assumed distances ranging between $D = 380$ pc, following our discussion in Paper I and in order to ease the comparison with our results in that paper, and 710 pc, as proposed by Men'shchikov et al. (2002). In Sect. 4.2 and Table 1, we give the scaling of our results with the distance.

Our accurate mapping of the Red Rectangle shows, just from inspection of the velocity–position diagrams, that the velocity field corresponds to Keplerian rotation. Our models confirm the presence of stable Keplerian rotation, at least in the inner regions of the disk, up to $\sim 8.5 \times 10^{15}$ $(\frac{D({\rm pc})}{710})$ cm. From this Keplerian rotation law we derive a total central mass (around which the gas disk rotates) of about 0.9 $M_\odot$, for $D = 380$ pc, and of ~ 1.7 $M_\odot$, for $D = 710$ pc (Sect. 4.2). Both values are within the range given by previous studies of the central binary system, including discussion of the dynamics and evolutionary state, and of their close environments (Men'shchikov et al. 2002; Waelkens et al. 1996), but the higher values of the mass (and distance) seem to be favored by the existing information (Sect. 4.2).

The presence of slow radial expansion in the outer disk is deduced from the absorption dip observed at slightly negative velocities. In these regions, the disk is still rotating, but with $V_{\rm t} \propto 1/r$, i.e. following the law of angular momentum conservation, as expected in the presence of expansion. In our best fitting, the expansion velocity in these outer regions decreases from about 1.6 km s^{-1} (at 8.4×10^{15} cm from the center) down to about 0 km s^{-1} (at the end of the CO disk). These values of the expansion velocity are slightly higher than those found in Paper I, since a faster expansion helps to fit some other minor features (Appendix A.2).

We note that some earlier investigations of the Red Rectangle have made use of the total CO profile width to derive an expansion velocity (values of 6–7 km s^{-1} were found) and kinematical times. This is clearly not justified in this case, since most of the CO line width comes from the rotation, and the molecular gas expands at much smaller velocities (regardless of the poorly known kinematics of the optical nebula).

A local turbulence velocity of about 0.3 km s^{-1}, in any case <0.5 km s^{-1}, is also deduced from the fitting. Note the particularly low turbulence present in this source.

CO is detected up to an outer disk radius $\sim 2.7 \times 10^{16}$ cm (for $D = 710$). The detection of CO emission at velocities as high as ±6 km s^{-1}, with respect to the systemic velocity (and assuming the above velocity law and distance), implies that we are probing gas in regions at about 6×10^{14} cm from the central star(s). Our observations do not probe CO-rich gas in still inner regions and, of course, do not serve to estimate their properties. In particular, we cannot try to compare our disk model with the very small central disk that is found to collimate the stellar light (Men'shchikov et al. 2002; Tuthill et al. 2002; Cohen et al. 2004).

The temperature and density of the disk are also deduced from our model. The temperature is well measured from the maps of the opaque $J = 2$–1 line. We find that the temperature decreases with the distance to the center following the law $T \propto 1/r^{0.7}$, see Table 1. T ranges between about 400 K (at $r \sim 6 \times 10^{14}$ cm) and about 30 K at the outer measured radius, 2.7×10^{16} cm.

In our previous observations (Paper I), the density was poorly measured because of the high opacity of the CO $J = 2$–1 transition and the low dynamic range of the $J = 1$–0 data. Our present data yield accurate maps of this line, allowing a reasonable study of the density distribution in the molecular disk. In any case, the $J = 1$–0 line is slightly opaque and the dependence of the observables on the density is only moderate;

therefore the accuracy of the density measurements remains lower than for the other parameters (Appendix A.4). Our best fitting is attained assuming a jump by a factor of 3 in the density between the inner region, in Kepler-like rotation, and the outer one, in which a slow expansion appears; we recall that the separation between both regions takes place at a distance from the center $R_{\rm kep} \sim 8.4 \times 10^{15}$ cm. In both regions the density decreases approximately with the square radius. Although the overall values of the density are only certain within a factor ∼2, the comparison of data and model predictions indicates, with a reasonable degree of confidence, that there is a strong decrease in the density at the point at which the velocity regime changes ($R_{\rm kep}$) or just after it.

The total mass of the model disk is 2×10^{-3} $M_\odot$ (3.5×10^{30} gr) for $D = 380$ pc, and 6×10^{-3} $M_\odot$ for $D = 710$ pc. As seen, our CO 1–0 data limit the opacity in this line, leading to lower densities and total mass than those taken in Paper I. The total mass is, however, larger than that obtained from single-dish data of CO $J = 2$–1 by Bujarrabal et al. (2001); the reason is that now we can use a less opaque line and a well measured (higher) temperature. See further discussion in Appendix A.

The laws and characteristic values of the density and temperature found in the rotating disk around the Red Rectangle are quite similar to those typical of circumstellar envelopes around AGB stars, but different from those of the bulk of the molecular gas in most PPNe (which show significantly lower temperatures, ∼15 K, and higher total masses, $\gtrsim$0.1 $M_\odot$). We recall that, in any case, the molecular gas disk in the Red Rectangle is very different from AGB envelopes in structure and kinematics: AGB shells in general show overall spherical shapes, fast expansion (∼10 km s^{-1}), and no obvious signs of rotation.

The presence of a rotating disk may be one result of the binary nature of the central star of the Red Rectangle, being perhaps absent or much less prominent in most PPNe. But we cannot discard the possibility that such disks are a common phenomenon in PPNe, although often more difficult to detect, explaining the bipolar energetic jets characteristic of these objects (Sect. 1). We note that existing molecular observations are often not conclusive in this respect, because of the probable small size and velocity dispersion of the disk and confusion with the strong, extended CO emission of many PPNe.

Acknowledgements. This work was supported by the Spanish Ministerio de Ciencia y Tecnologia and European FEDER funds, under grants AYA2000-0927, ESP2001-4519-PE and ESP2002-01693. A.C.-C. was supported during the development of this work by a Marie-Curie Intra-European Fellowship within the 6th European Community Framework Programme. We are grateful to C. Waelkens, non-anonymous referee of this paper, for his stimulating comments.

References

Alcolea, J., & Bujarrabal, V. 1991, A&A, 245, 499
Bujarrabal, V., Alcolea, J., Neri, R., & Grewing, M. 1997, A&A, 320, 540
Bujarrabal, V., Alcolea, J., & Neri, R. 1998, ApJ, 504, 915
Bujarrabal, V., Castro-Carrizo, A., Alcolea, J., & Sánchez Contreras, C. 2001, A&A, 377, 868
Bujarrabal, V., Neri, R., Alcolea, J., & Kahane, C. 2003, A&A, 409, 573 (Paper I)
Castro-Carrizo, A., Bujarrabal, V., Sánchez Contreras, C., Alcolea, J., & Neri, R. 2002, A&A, 386, 633
Cohen, M., Van Winckel, H., Bond, H. E., & Gull, T. R. 2004, AJ, 127, 2362
Frank, A., & Blackman, E. G. 2004, ApJ, 614, 737
Goldreich, P., & Scoville, N. 1976, ApJ, 205, 144
Groenewegen, M. A. T., Van der Veen, W. E. C. J., & Matthews, H. E. 1998, A&A, 338, 491
Jura, M., Balm, S. P., & Kahane, C. 1995, ApJ, 453, 721
Jura, M., Turner, J., & Balm, S. P. 1997, ApJ, 474, 741
Jura, M., & Kahane, C. 1999, ApJ, 521, 302
Lopez, B., Mékarnia, D., & Lefèvre, J. 1995, A&A, 296, 752
Mamon, G. A., Glassgold, A. E., & Huggins, P. J. 1988, ApJ, 328, 797
Men'shchikov, A. B., Schertl, D., Tuthill, P. G., Weigelt, G., & Yungelson, L. R. 2002, A&A, 393, 867
Roddier, F., Roddier, C., Graves, J. E., & Northcott, M. J. 1995, ApJ, 443, 249
Schöier, F. L., & Olofsson, H. 2001, A&A, 368, 969
Soker, N. 2002, ApJ, 568, 726
Tuthill, P. G., Men'shchikov, A. B., Schertl, D., et al. 2002, A&A, 389, 889
Waelkens, C., Van Winckel, H., Waters, L. B. F. M., & Bakker, E. J. 1996, A&A, 314, L17
Waters, L. B. F. M., Trams, N. R., & Waelkens, C. 1992, A&A, 262, L37
Zweigle, J., Neri, R., Bachiller, R., Bujarrabal, V., & Grewing, M. 1997, A&A, 324, 624

Online Material

Appendix A: Reliability and uniqueness of the model fitting

The values derived from our model fitting for the free parameters discussed in Sect. 4 present different degrees of confidence, depending on how strongly the observational features depend on them. We first analyze the geometrical and kinematical parameters, which are more directly related to the data; the rest of the discussion will assume that geometry and kinematics are fixed.

The uncertainties in the parameter values given in the following discussions take the uncertainties in the calibration of the data into account along with some allowed differences between the model predictions and the observed maps. We note that the value ranges given in the following subsections, as allowed by the fitting process, apply to the typical values on the whole disk, since the physical conditions vary across it.

In general, we assume distances D between 380 and 710 pc in our modeling. The scaling of the fitted values with the distance is discussed in Sect. 4.2.

A.1. Size and general structure

As seen (Sect. 4.1), the main parameters of the disk structure are quite directly deduced from the maps themselves. The outer radius of the CO emitting disk $R_{\rm out}$ is well measured (for our sensitivity level) and can vary by only ∼10%. We note (Fig. 3) that the observed radius of the disk is slightly larger toward positive offsets (i.e. toward the east) than in the opposite sense. This may be due either to the radius of the disk not being constant or to its inner and outer parts not having the same centroid. We prefer to keep the simplicity of the model and this difference is not reproduced in our predicted maps, which are symmetric in that respect. The direct measurements of the disk width H are, however, uncertain and their interpretation depends significantly on the contribution of the size of the disk projection on the plane of the sky, as well as on possible warps or asymmetries.

A.2. Velocity field

Although infinite combinations of rotational and expansion velocities can be imagined, the extensive information on the velocity field contained by our high-quality observations is very restrictive in this respect.

We assume that two velocity regimes are present in the gas disk, with Keplerian rotation in its inner parts and rotation plus slow expansion in outer regions. As we mentioned in Paper I and again in Sect. 3, the presence of expansion in the outermost regions is necessary to explain the selfabsorption found at velocities between ∼0 and −1.5 km s^{-1} LSR, which results in lower brightness temperatures than at the corresponding positive velocities. A purely rotating disk cannot yield such a feature, resulting in velocity–position diagrams that are practically symmetric by inversion around the central velocity and position. In this outer region we also assume that the tangential velocity varies following $V_{\rm t} \propto 1/r$.

Our model confirms that a single rotational velocity field across the whole disk is not compatible with our data. See in Fig. A.1 the predictions by models in which the rotational velocity follows the same law in the whole disk, varying with $1/\sqrt{r}$ (Keplerian rotation) and with $1/r$ (angular momentum conservation), respectively. In both cases, we keep a low expansion velocity in the model, although the composition of Keplerian rotation and expansion does not seem to have a physical meaning, since Keplerian rotation is only expected in very stable systems (if expansion appears, one expects the rotational velocity to vary more or less proportionally to $1/r$).

As we see in Fig. A.1, the first case (Keplerian rotation in all the disk) leads to too big a separation in velocity of the outskirts of the disk, due to the slow decrease in velocity. The second case ($V_{\rm t} \propto 1/r$ everywhere) leads to too large a separation in position of the regions emitting at the extreme velocities, because the velocity becomes very high in the inner disk regions, while in the observations they are practically coincident. We note that in both cases we allowed the density and temperature to vary, still trying to fit the data. We think, from our calculations, that the presence of Keplerian rotation of the inner disk regions and of a slow expansion in the outer ones is unavoidable.

The value of $R_{\rm kep}$, the distance at which both regimes are separated, is however not very well determined. We find that the predictions may still be compatible with the observations for variations of $R_{\rm kep}$ by a factor $\lesssim$1.5, provided that $V_{\rm t}(R_{\rm kep})$ and the density and temperature parameters vary accordingly to maintain the overall values of $V_{\rm t}$, n, and T. The predictions in the extreme cases are, in any case, clearly less similar to the observations than for our standard model.

A total central mass ∼1.7 $M_\odot$ (for D = 710 pc) is directly derived from the parameters defining the Keplerian rotation. The total central mass is slightly affected by the uncertainty in $R_{\rm kep}$, since, as we have seen, $V_{\rm t}(R_{\rm kep})$ must change when we consider different values of $R_{\rm kep}$. On the other hand, we note the strong dependence of the mass on the rotational velocity, as $V_{\rm t}^2$. From the acceptable values of the Keplerian velocity field, we estimate that the uncertainty of the central stellar mass is smaller than ∼30%. We note that the rotation velocity field deduced here is very similar to the best fitting in Paper I (model B).

As mentioned, the asymmetry in the velocity profiles, with an "absorption-like" feature at slightly negative velocities, can be explained assuming a low expansion velocity at distances larger than $R_{\rm kep}$. The best fitting is obtained if $V_{\rm exp}$ decreases from $R_{\rm kep}$ outwards, from 1.6 km s^{-1} to ∼0 km s^{-1}. We choose a law $V_{\rm exp}(r) = \sqrt{a + b/r}$, expected for a force field varying with $1/r^2$ (as gravitational and radiation pressure forces, under simplifying assumptions); a simple linear law for $V_{\rm exp}(r)$ with the same extreme values leads to very similar results.

The values of $V_{\rm exp}$ in our present work are somewhat higher than those deduced in Paper I (0.55 km s^{-1}). This is the most important difference in the velocity field deduced in both works. The reason for the change in the expansion is that our present maps clearly confirm the main observational feature that remained unexplained by the model published in 2003: the presence of weak emission at positive/negative relative

velocities from negative/positive offsets along the disk direction. We have found that, within the frame of our simple model, only a moderate increase of the expansion velocity of the outer layers can significantly improve the fitting of these features. When $V_{\rm exp}$ is comparable to $V_{\rm rot}$, the composition of expansion and rotation at about 8.5×10^{15} cm may inverse the sign of the velocity projected in the line of sight, with respect to the case of pure rotation, leading to the observed features. In any case, the fitting is still not perfect; as we can see in Fig. 5 some small residuals appear, as for instance the too negative velocity of the maximum at about -2 km s^{-1} LSR and some emission excess at $\sim$(+2 km s^{-1}, +1″) and (+0.5 km s^{-1}, −1″). Some of these errors result precisely from the too sudden increase of $V_{\rm exp}$ at $r = R_{\rm kep}$; but they are, in any case, much smaller than the residuals if a value of $V_{\rm exp}$ similar to that in Paper I is used. We show our best fitting for a constant expansion velocity in Fig. A.1: $V_{\rm exp} = 0.6$ km s^{-1}, the other parameters being quite similar to those of our standard model. Note the too sudden decrease in the model nebula emission at positive/negative relative velocities from negative/positive offsets along the disk direction; on the other hand, some of the small residuals mentioned above are slightly less noticeable.

The value found for the local turbulence, $\sigma_{\rm turb} \sim 0.3$ km s^{-1}, mainly has a cosmetic effect on the synthetic maps. Less neat predictions, but still compatible with our data, are produced for $\sigma_{\rm turb}$ ranging between 0 and 0.4 km s^{-1}. We note that similar results can be produced if we assume, instead of a local and constant turbulence, departures from the macroscopic velocity field (within a dispersion of the order of 0.3 km s^{-1}) or from the disk geometry (like undulations or warps). Values of $\sigma_{\rm turb}$ larger than 0.4 km s^{-1} produce velocity dispersions in the outer disk that are much too wide and incompatible with the observations

A.3. Temperature, T

The values of the characteristic temperature (see definition in Sect. 4.1) are relatively well measured, since the brightness of the opaque $J = 2$–1 line at the different positions and projected velocities is mainly given by the temperature of the different components. We estimate that variations larger than 20% in most of the nebula are not compatible with the observations, within the restrictions mentioned at the beginning of the subsection, in particular for the assumed source shape. The uncertainty related to the emitting region size is particularly important in the very inner regions, whose thickness remains poorly known.

The temperatures deduced here are comparable to those found in AGB envelopes but significantly higher than those usually found in molecule-rich gas in PPNe, ∼15 K (see e.g. Bujarrabal et al. 2001). Higher values in the Red Rectangle are imposed by the measured brightness temperatures, sometimes over 50 K. Our temperature law is in general quite similar to that deduced in Paper I.

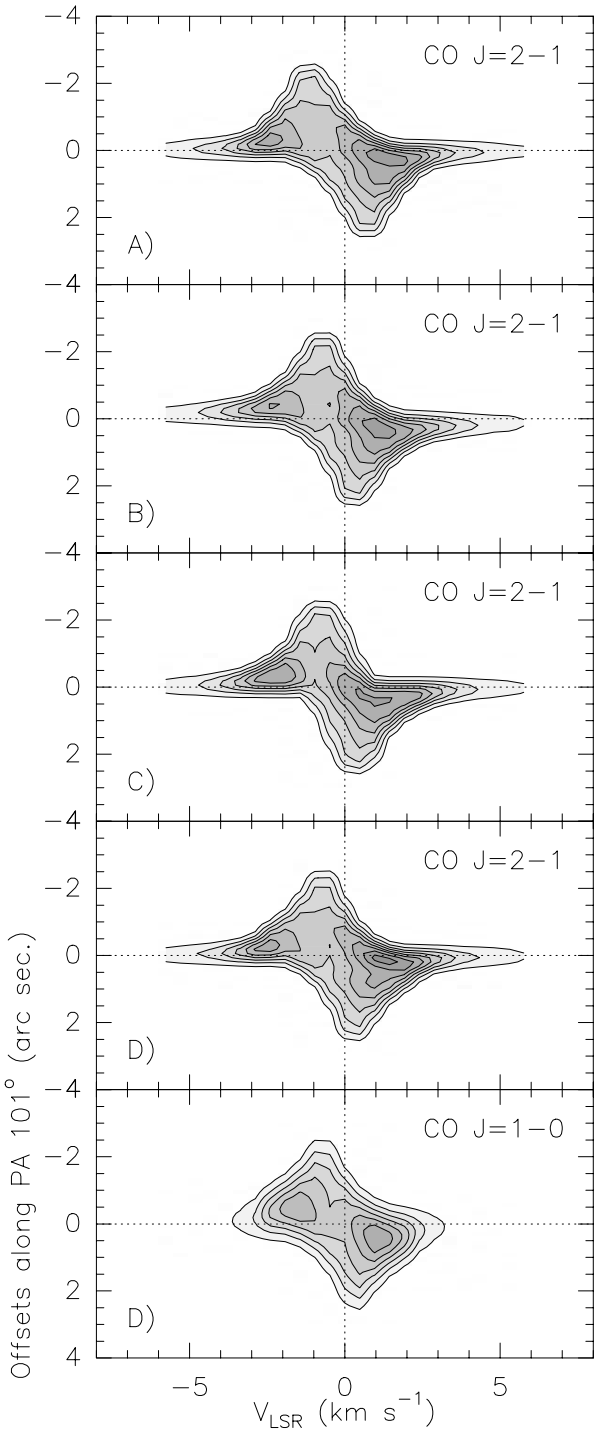

Fig. A.1. Synthetic velocity–position diagrams along the direction of the CO disk for models in which we have chosen combinations of the parameters different from those of our best fitting. Contours are as in Fig. 3. These predictions are considered to be less accurate by comparison with the data, see Appendix A. From top to bottom: **A)** Rotational velocity varying as $V_{\rm t} \propto 1/\sqrt{r}$ (Keplerian) in the whole disk. **B)** $V_{\rm t} \propto 1/r$ (angular momentum conservation) in the whole disk. **C)** Constant expansion velocity, $V_{\rm exp} = 0.6$ km s^{-1}, in the outer disk. **D)** No jump in the density at $r = R_{\rm kep}$, but strong decrease from this point (Appendix A.4).

A.4. Density, n

It is very difficult to measure the density from the $J = 2$–1 maps, since this line is very optically thick in most of

the lines of sight. The J = 1–0 line is only moderately opaque, and the comparison of its maps with the predictions are more useful in this respect, although the dependence of the intensities on the density values is still low. The key observational datum in this case is the relatively weak emission from the outermost parts of the disk in this line (Figs. 2, 3), which implies that CO J = 1–0 is not optically thick in these regions. If the rest of the parameters are kept constant (in particular the CO abundance, see next subsection), overall variations of the density values by a factor >2 are not allowed. As for the temperature, the density of the innermost regions is particularly uncertain, because of their unknown extent.

If the jump factor of the densities at the Keplerian radius $R_{\rm kep}$ disappears, the fitting is worse, though perhaps acceptable (Fig. A.1). In this model the density at $R_{\rm kep}$ is equal to 2.8×10^5 cm^{-3}, and we must introduce a strong decrease of the density farther than $R_{\rm kep}$, with α_n = 3.5, which in some way mimics the jump in density of our standard fitting. The temperature of the Keplerian region is also different in this model, with $T(R_{\rm kep})$ = 50 K and $\alpha_{\rm T}$ = 1.

We note that the densities and total mass derived here are somewhat smaller than those given in Paper I. As mentioned, our CO 1–0 data limit the opacity in this line, leading to lower densities and total mass than those assumed in that work. The total mass remains, however, larger than that obtained from single-dish data of CO J = 2–1 by Bujarrabal et al. (2001); the reason is that this line is very probably opaque and that we assumed too low temperatures in 2001, those usual in PPNe, while the data in this paper indicate temperatures that are on average ∼4 times higher (A.3).

A.5. CO abundance, X(CO)

As we have mentioned, the density and the CO relative abundance can vary in opposite senses without affecting the model results, provided that the product nX(CO) remains constant. Therefore, the discussion of X(CO) requires other arguments than strictly the agreement between model predictions and observations. We adopted a value $X(\mathrm{CO}) = 2\times10^{-4}$, according to the results usually found in PPNe (Sect. 4.1).

Single-dish (unpublished) observations made with the IRAM 30-m telescope indicate that the ^{12}CO/^{13}CO J = 1–0 line intensity ratio is low, ∼2.4. A somewhat smaller ratio is found for the J = 2–1 line. Similar line intensity ratios are often found in PPNe (e.g. Bujarrabal et al. 2001). This indicates that the CO emission in the Red Rectangle is, from the point of view of the intensity and opacity, not very different from those in other PPNe. In particular, a relatively low $X(^{12}\mathrm{CO})/X(^{13}\mathrm{CO})$ is suggested.

A much higher value of $X(^{12}\mathrm{CO})$ is not expected, in any case, since the total mass derived for the gas disk in the Red Rectangle is already very low for a PPNe. Moreover, CO abundances larger than $\sim5\times10^{-4}$ are not found even in the inner layers of the envelopes around AGB stars (as an example of very molecule-rich gas). Significantly smaller values are thought to be possible if photodissociation from the interstellar radiation field is important (note that the central star of the Red Rectangle is quite cool). But in this case, the photodissociation easily becomes very efficient and CO is fully destroyed in a short time (e.g. Mamon et al. 1988); so that intermediate values of X(CO), much lower than 10^{-4} but not negligible, are very improbable.